LASER THERMOMECHANICAL EVALUATION OF BONDING INTEGRITY

H. I. Ringermacher, B. N. Cassenti, J. R. Strife and J. L. Swindal

United Technologies Research Center
East Hartford, CT 06108

INTRODUCTION

Thermal imaging for the nondestructive evaluation (NDE) of materials appears to be of ever increasing importance for industrial applications. The development of new materials, both metallic and ceramic, as thermal and oxide barrier coatings present new challenges to inspection techniques. Thermal imaging methods seem ideally suited for such applications, being particularly sensitive to surface and near surface material thermal inhomogeneities that may be defect-related. However, these same sophisticated materials can pose rather sever requirements upon the efficacy of any particular type of thermal imaging. Typical problems encountered include rough, optically scattering surfaces, surfaces ranging from highly reflective to absorptive, complex surface geometry and microscopic to very macroscopic (practical components) imaging requirements.

Thermal techniques include both photo-thermal and photoacoustic imaging. Infrared camera methods can image subsurface defects in both metal and insulating coatings and have the advantage that large areas can be covered quickly [1, 2]. These methods, however, fail to provide any indication of the mechanical coupling of the coating to its substrate. Even a fully disbonded coating in good touch contact with its substrate will appear bonded thermally since the thermal resistance at such an interface is very low.

Thermomechanical Imaging

Recently, a new contrast mechanism, thermomechanical imaging, has been developed. This provides, for the first time, the ability to visualize the mechanical properties of an interface and thus has application to coating adherence and bonding of thin sheets and plates to substrates. Thermomechanical imaging can display a graded image of coating adherence from good bond to total disbond. The method works by thermally stressing the surface with the input laser beam and monitoring the resultant sound transmission, via mechanical coupling to the substrate, with the laser interferometer. A weak acoustic response is representative of a poor mechanical coupling at the interface. Successful applications include evaluation of ceramic coatings on metal substrates, aluminide coatings on metals, ceramic coatings on carbon/carbon composites, subsurface defect detection in both metals and ceramics and thermomechanical evaluation of electronic materials and components.

PHOTOACOUSTIC SYSTEM

Figure 1 shows the experimental arrangement of the laser heating source together with the Doppler heterodytne interferometer detection and computer control system. A typical power level is 200–500 mW to the target from the argon laser. The beam is modulated at the desired photoacoustic frequency up to 100 kHz. This excites an acoustic response in the specimen which

Review of Progress in Quantitative Nondestructive Evaluation, Vol. 9
Edited by D.O. Thompson and D.E. Chimenti
Plenum Press, New York, 1990

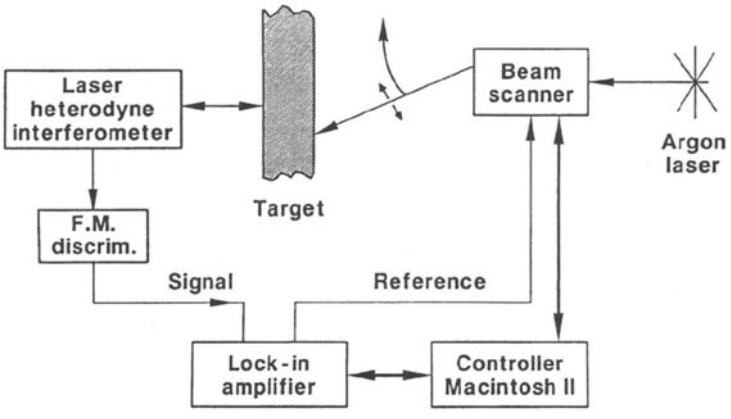

Figure 1. Block diagram of photoacoustic laser scanning and interferometer detection system.

is detected by a laser Doppler interferometer sensitive to surface velocity. The modulated beam is then raster scanned over the specimen with galvanometer mirrors at a rate of up to 10 mm/sec. A typical image coverage would be a 25 mm x 25 mm area with 50 micron resolution in approximately 10 minutes. Finer resolutions are achievable at the cost of increased scanning time. As a rule, the resolution of thermomechanical imaging is approximately equal to the depth of the imaged defect below the surface. For example, a 100 μm wide defect located 200 μm below the surface will appear at least 200 μm wide in the image. Thus, it is most efficient to scan at a rate providing this minimum resolution.

Beam modulation can be either intensity or coordinate modulation. Intensity modulation is the standard technique. Coordinate modulation (CM) involves dithering the beam slightly in the direction of the scan. This has the effect of producing a spatial signal–difference image. Its advantage is an improvement of image contrast and signal/noise ratio. Coordinate modulation is discussed more extensively in Refs.[3, 4]. Both techniques have been used in the present work.

During examination, the specimen is held at the edges so as to obtain, as closely as possible, a simply supported boundary condition. The interferometer can be focused almost anywhere on the back or front side of the specimen except too close to support points. The Doppler heterodyne interferometer is discussed in Ref. [5].

Often, upon excitation of the specimen by the modulated laser beam, natural specimen mechanical resonances can be found. It is advantageous to operate the modulation at these discrete frequencies, as convenient, in order to take advantage of the typical "Q–enhancement" effects which may improve SNR a hundred–fold or more. This was done for much of the work presented. Since a number of resonances are typically available, the frequency closest to that physically desirable (for example to limit thermal penetration depth) is chosen. Frequencies used cover 1 kHz – 20 kHz. The CM technique suppresses the slowly–varying spatial modes, compared to the high spatial frequency defect images, by a simple adjustment of the peak–to–peak dither spacing on the target at approximately the defect size.

The modeling that follows simulates the above process as closely as possible. Results of the CM technique applied in the modeling are also presented.

THEORETICAL MODELING

The thermomechanical mechanism has been observed experimentally [6] and modeled using finite elements with excellent agreement [7]. In this work, we present analytic modeling

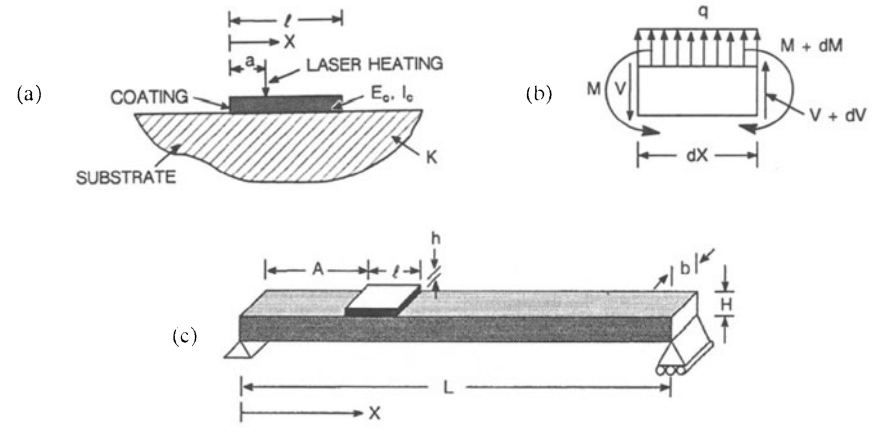

Figure 2. Thermomechanical beam model used for the analysis.

and compare it with observation on plate bonding applications such as silicon nitride coatings on carbon/carbon (C/C).The modeling is then used to assist in qualitative image interpretation on other bonded systems. Silicon nitride coatings microcrack naturally on high modulus C/C substrates due to thermal expansion mismatch stress buildup following deposition. This model simulates the thermomechanical response of a coating segment to a laser beam scanned from one edge to the other. The laser beam heats a small scanned spot on the surface which provides a time dependent thermal load to the coating segment at the laser beam modulation frequency. The coating segment is modeled as being perfectly attached to an elastic foundation, here approximated as a beam. The thermal load then bends the beam and this deflection is monitored by a laser interferometer at a fixed point on the surface. The frequency is kept below any fundamental modes of the sample and the resultant response is phase-coherently detected so that a static elastic model is adequate. This is feasible because a typical acoustic wavelength is on the order of a meter while a specimen dimension is several centimeters. The theory predicts a deflection response for a perfectly attached coating with known thermoelastic properties which is then compared to the observed response in a real specimen. A disbond or weak bond will show as a deviation from the predicted scan response.

Mechanical Response of a Coated System

The mechanical response of a coated beam will be described as a combination of two models. In Fig. 2 the coating response is modeled as a beam on an elastic foundation. The model is completed by considering the response of the substrate to the forces induced by the coating.

Following the description in Ref. 8 the moment on the coating is (Fig. 2a)

$$M = \int_{-h/2}^{h/2} \sigma b z \, dz \quad , \tag{1}$$

where σ is the stress in the coating, and z is the vertical distance from the central plane of the coating.

From Hooke's law we use

$$\sigma = E_c(\epsilon - \alpha_c T) \quad , \tag{2}$$

where E_c is Young's Modulus for the coating, α_c is the coating coefficient of thermal expansion,

and T is the rise in temperature. Then since the strain is given by

$$\epsilon = -z\frac{d^2w_c}{dx^2} \ , \tag{3}$$

where w_c is the coating deflection, the moment becomes

$$M = -E_cI_c\frac{d^2w_c}{dx^2} - M_T \ . \tag{4}$$

$I_c = bh^3/12$ is the cross-sectional moment of inertia, and

$$M_T = \alpha_cE_cb\int_{-h/2}^{h/2} Tz \ dz \ . \tag{5}$$

Equilibrium [8], seen in Fig. 2c, can be used to show

$$\frac{d^2M}{dx^2} = \frac{dv}{dx} = -q \ . \tag{6}$$

From Fig. 2a, the transverse force is

$$q = -K_sw_c \ . \tag{7}$$

Equations (4), (5) and (6) yield the governing equation:

$$E_cI_c\frac{d^4w_c}{dx^4} + K_sw_c = -M_0\delta''(x-a) \ ,$$

where

$$\delta'' = \frac{d^2\delta}{dx^2} \ , \tag{8}$$

and we have used a concentrated moment $M_T = M_0\,\delta\,(x-a)$ where δ is the Dirac delta function.

From Fig. 1 the boundary conditions are given by a vanishing shear, V, and moment, M, at the ends. From Eq. (6) these become:

$$\frac{d^2w_c}{dx^2} = o \qquad @x = o, \ell \ , \tag{9}$$

$$\frac{d^3w_c}{dx^3} = o \qquad @x = o, \ell \ . \tag{10}$$

The δ function in Eq. 8 can be eliminated by defining a new displacement function,

$$W_c = w_c + \frac{M_0}{E_cI_c} < x-a > \tag{11}$$

and the unit ramp function <x–a> is defined from:

$$< x > \ = \begin{cases} o & x < o \\ x & x \geq o \end{cases} \ . \tag{12}$$

Then the governing equation becomes

$$\frac{d^4W_c}{dx^4} + 4k^4W_c = 4k^4M_o < x-a > \ , \tag{13}$$

where

$$4k^4 = \frac{K_s}{E_c I_c} \quad . \tag{14}$$

The substrate stiffness K_s is given by:

$$K_s = \frac{E_s b}{H} \quad . \tag{15}$$

From this and (14) we can define a "normalized system stiffness", K, from

$$K = k\,\ell = \left(\frac{3\ell^4 E_s}{h^3 H E_c}\right)^{\frac{1}{4}} \tag{16}$$

which is a quantity characterizing the system response. A stiff substrate is equivalent to a strong bond and a sharp response as the laser beam enters or leaves the coating surface. A weaker bond will have smaller values of K producing or spread in the response.

The displacement response of the substrate is required to complete the model. The analysis is, however, similar to that for the coating beam model. Boundary conditions on continuity of displacements and slopes as well as reaction force balance must be applied. Details of these calculations are presented elsewhere [9].

Figure 3 shows the results of these calculations as applied to the CM technique which is essentially imaging the slope of the substrate displacement response W_s. The K=100 response corresponds in reality to an unrealistic extremely stiff system. The K=10 response is approximately that predicted for silicon nitride on carbon/carbon (K=12) for coating segments of dimensions shown in Figure 4. The K=1 response would be representative of a poor coating–substrate coupling, that is, a soft bond. Thus when actual data are compared and deviate from the "perfect bond" case, we may assume that the deviation arises from failure of the "perfect attachment" assumption with resultant responses given by the "soft bond" predictions. This is actually found and is described in the remaining sections.

APPLICATION AND RESULTS

Figure 4a shows a Scanning Electron Microscope image of a microcracked silicon nitride coating on a carbon/carbon substrate. Figures 4b–4d show the results of a single laser beam scan through the large central coating segment. Figure 4b is a laser thermomechanical image of the silicon nitride coating with a single white line superimposed where the single scan line data was taken. The experimental scan response from left to right on the large coating segment (Fig. 4c) compares favorably with the K = 10 theory case (Fig. 4d) indicating a good bond and valid thermomechanical modeling. Coordinate modulation was used in this example.

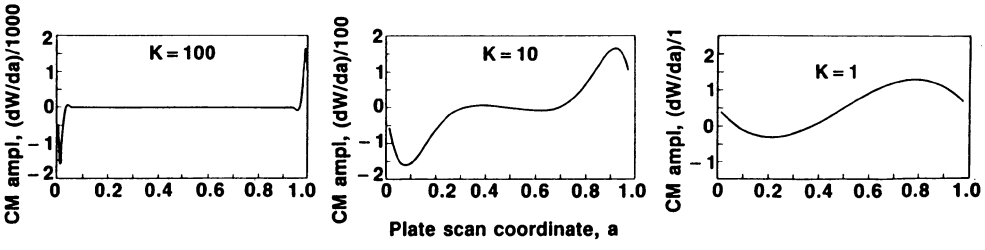

Figure 3. Thermomechanical modeling results showing the deflection responses of the substrate to a single scan line over the coating.

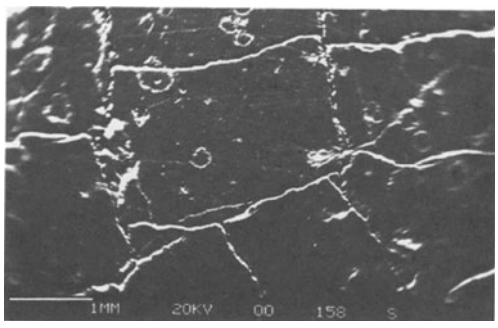

(a)

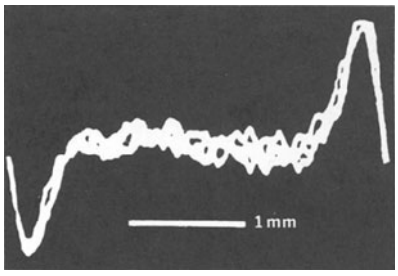

(c)

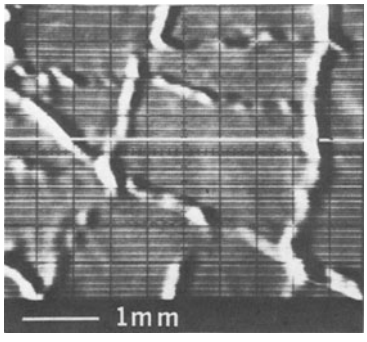

(b)

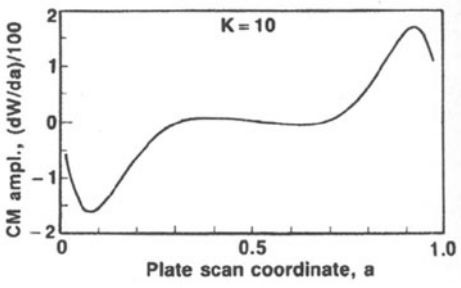

(d)

Figure 4. Comparison of experiment and theory for the thermomechanical response of silicon nitride on C/C.

The use of zirconia thermal barrier coatings on nickel alloy substrates is an important engineering application. Shown in Figure 5a is such a coating approximately 0.25 mm thick on a one-half inch rod specimen which has been exposed in a high temperature burner rig resulting in ablation and partial disbonding. The purpose of the thermomechanical evaluation was to determine the extent of disbonding beyond the ablated regions and to follow the progress of disbonding as the thermal exposure continued. The thermomechanical image of the same region obtained with the above noncontact laser technique is shown in Figure 5b. A 1 kHz frequency was used along with 1 watt of laser scanning power. Approximately 10 mm square was imaged with the interferometer sensor focused at a fixed point on the rod, which had to be carbon coated for inspection due to the exceptionally high reflectivity of the zirconia for green argon light. The ablated, bare metal black area (a) and totally disbonded white areas (b) are clearly seen. In addition, it is evident that at least two other regions stand out: areas (c) are well bonded and remained intact during the thermal exposure while areas (d) show partial disbonding, indicated by white blotchy zones. These areas are of greatest interest since, apparently, this is where disbonding initiates. The image clearly shows bond compliance variation everywhere and thus can be useful in interpreting bond strength.

Applications to electronic materials are also very promising. The thermomechanical technique has been applied to evaluation of bond integrity for electrostatically bonded silicon wafers. Figure 6a is a photo taken of an etch pattern showing a 25-device array on the face of a 1.2 mm thick, 37 mm square silicon wafer prior to bonding to a 0.2 mm thick wafer. The pattern incorporated intentional disbonds 0.2 mm, 0.6 mm and 1.5 mm wide placed at various points around a device as well as on random devices on the wafer. The 0.2 mm disbond was chosen to be equal to the top plate thickness since this was the expected resolution limit according to the thermomechanical analysis.

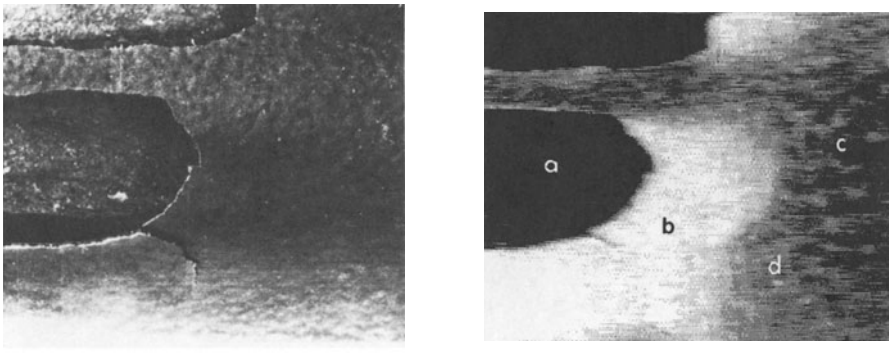

(a) (b)

Figure 5. Thermomechanical image of a zirconia coating on a nickel alloy substrate.

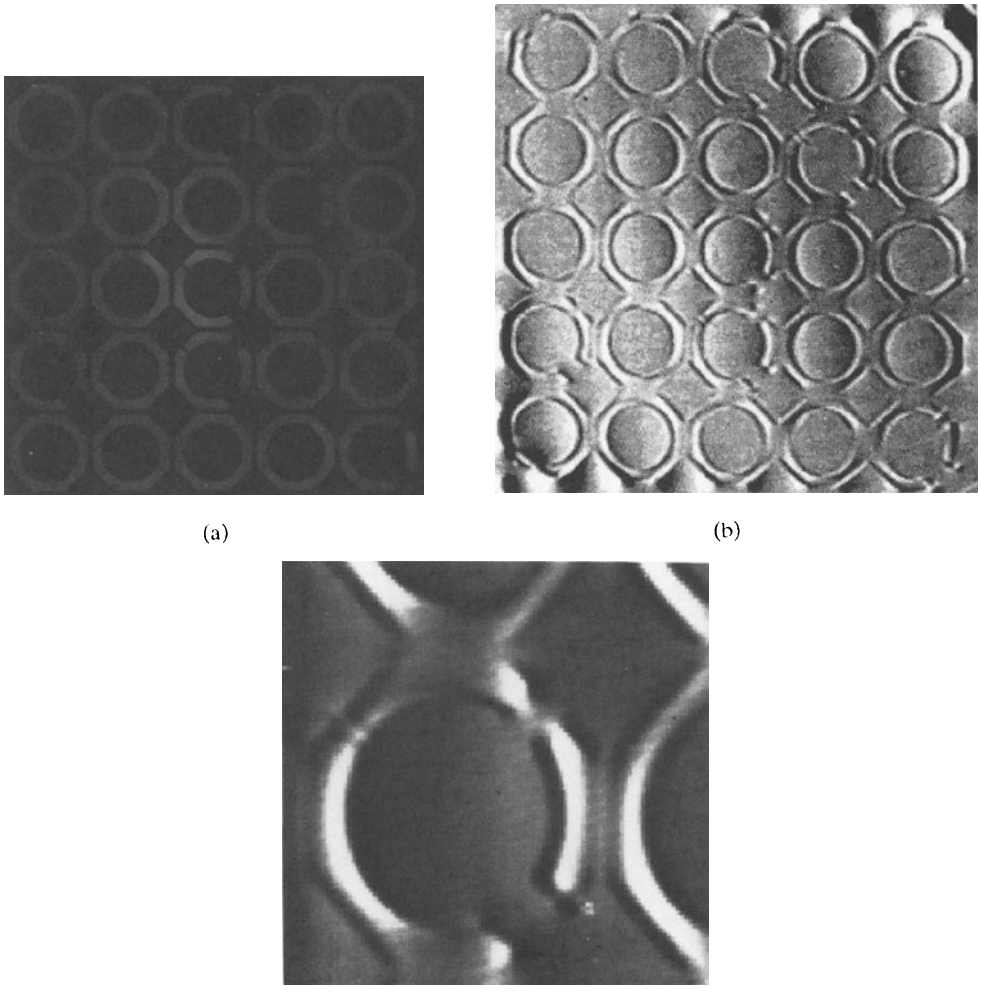

(a) (b)

(c)

Figure 6. Thermomechanical images of an array of devices at the bondline between two silicon wafers.

Figure 6b shows the thermomechanical image of the bond interface, after bonding, resulting from raster scanning the argon laser beam over the thin wafer face while detecting the bonded wafer response with the laser interferometer focused at the thicker back side center. The wafer was held lightly at the edges with minimal contact. The modulation frequency chosen was at a natural plate resonance near 10 kHz resulting in a thermal diffusion length of approximately 0.02 mm. This choice permitted the thermomechanical mechanism to dominate the bondline image since the thermal wave could not penetrate the necessary 0.2 mm depth. All intentional defects are clearly indicated along with some unintentional ones such as those seen on the lowest left and top left devices as well as the presence of a dust particle in the gap of the uppermost right device. The scan took approximately 10 minutes to complete with a 0.2 mm scan resolution and 0.12 mm laser spot size. Approximately 80 mW of laser power was absorbed by the wafer for the image with insignificant temperature rise and no damage.

Figure 6c shows a separate scan of a single device with a greater scanning resolution of 0.07 mm. The 0.2 mm disbond is indeed visible but not well resolved as predicted, thus further validating the thermomechanical mechanism.

SUMMARY

Noncontact laser thermomechanical NDE provides a visual image of bondline mechanical properties. The observed variation in bond compliance can be correlated to bond strength if the bonding failure mechanism is understood but at the very least can provide a continuous indication of bond integrity from total disbond to perfect attachment. Thermomechanical images generated by this method can be readily understood and interpreted since the supporting theoretical modeling has been confirmed experimentally several ways. Applications include ceramic coatings for oxidation and thermal barrier protection and bond evaluation for electronic materials. The technique seems particularly well suited for bond evaluation in thin layered structures and can be scaled in speed, resolution and required power according to the dimensions of the structure.

REFERENCES

1. P. K. Kuo, Z. J. Feng, T. Ahmed, L. D. Favro, R. L. Thomas: "Springer Series in Optical Sciences", 58, 415–418, Photoacoustic and Photothermal Phenomena, Editors, P. Hess and J. Pelzl, Springer–Verlag Berlin Heidelberg (1988).

2. L. J. Inglehart, E. H. LeGal–LaSalle: "Photothermal Characterization of Ceramics by Mirage Effect", Conference on NDT of High–Performance Ceramics, Boston MA, USA, August 25–27 (1987).

3. H. I. Ringermacher: "Coordinate Modulation Photoacoustics with Piezoelectric Detection", IEEE Ultrasonics Symposium, IEEE Cat. #82CH1823–4, 2, 576 (1982).

4. H. I. Ringermacher and C. A. Kittredge: "Photoacoustic Microscopy of Ceramics Using Laser Heterodyne Detection", Review of Progress in Quantitative Nondestructive Evaluation, 6B, 1231 (1987).

5. H. I. Ringermacher: "Laser Doppler Heterodyne Interferometer for Photoacoustic Applications", Ultrasonics International 87 Conference Proceedings, 165 (1987).

6. H. I. Ringermacher and L. Jackman: "Deep Thermoacoustic Imaging Using Scanning Electron Acoustic Microscopy", Review of Progress in Quantitative Nondestructive Evaluation, 5A, 567 (1986).

7. H. I. Ringermacher and M. Bak: "Thermomechanical Contract Mechanism in Thermoacoustic Imaging for NDE", Review of Progress in Quantitative Nondestructive Evaluation, 7A, 238 (1988).

8. B. A. Boley and J. H. Weiner: "Theory of Thermal Stresses", McGraw–Hill Book Co., NY, 1959.

9. H. Ringermacher and B. Cassenti: "Laser Thermomechanical Imaging of Coating/Substrate Systems", (to be published).